



HAL
open science

Variability of Sea-Surface Magnetic Anomalies at Ultraslow Spreading Centers: Consequence of Detachment Faulting and Contrasted Magmatism?

F. Zhou, J. Dyment

► **To cite this version:**

F. Zhou, J. Dyment. Variability of Sea-Surface Magnetic Anomalies at Ultraslow Spreading Centers: Consequence of Detachment Faulting and Contrasted Magmatism?. *Geophysical Research Letters*, 2022, 49, 10.1029/2021GL097276 . insu-03643048

HAL Id: insu-03643048

<https://insu.hal.science/insu-03643048>

Submitted on 18 Aug 2022

HAL is a multi-disciplinary open access archive for the deposit and dissemination of scientific research documents, whether they are published or not. The documents may come from teaching and research institutions in France or abroad, or from public or private research centers.

L'archive ouverte pluridisciplinaire **HAL**, est destinée au dépôt et à la diffusion de documents scientifiques de niveau recherche, publiés ou non, émanant des établissements d'enseignement et de recherche français ou étrangers, des laboratoires publics ou privés.

Copyright

Geophysical Research Letters[®]

RESEARCH LETTER

10.1029/2021GL097276

Key Points:

- The variability of sea-surface magnetic anomalies at ultraslow spreading centers reflects different degrees of magmatism along the ridge
- Gabbro bodies intruding the footwall of detachment faults partially record the magnetic polarity when this mode of spreading is active
- Sea-surface magnetic anomalies may represent a tool to estimate the spreading mode at ultraslow spreading centers

Supporting Information:

Supporting Information may be found in the online version of this article.

Correspondence to:

J. Dyment,
jdy@ipgp.fr

Citation:

Zhou, F., & Dyment, J. (2022). Variability of sea-surface magnetic anomalies at ultraslow spreading centers: Consequence of detachment faulting and contrasted magmatism? *Geophysical Research Letters*, 49, e2021GL097276. <https://doi.org/10.1029/2021GL097276>

Received 29 NOV 2021

Accepted 24 JAN 2022

Author Contributions:

Conceptualization: F. Zhou, J. Dyment

Formal analysis: F. Zhou

Investigation: F. Zhou

Methodology: F. Zhou, J. Dyment

Software: F. Zhou

Supervision: J. Dyment

Validation: F. Zhou, J. Dyment

Writing – original draft: F. Zhou

Writing – review & editing: J. Dyment

Variability of Sea-Surface Magnetic Anomalies at Ultraslow Spreading Centers: Consequence of Detachment Faulting and Contrasted Magmatism?

F. Zhou¹ and J. Dyment¹ 

¹Université de Paris, Institut de physique du globe de Paris, CNRS, Paris, France

Abstract The capacity of oceanic crust to record geomagnetic polarity reversals makes sea-surface magnetic anomalies an essential tool to study plate tectonics. The anomalies are usually well-defined at magmatic spreading centers, but are distorted and eventually disappear on magma-poor mid-ocean ridges such as the ultraslow Southwest Indian Ridge (SWIR), making their interpretation difficult. We attribute the variability of the SWIR sea-surface magnetic anomalies to the alternance of magmatic spreading and detachment faulting. A three-layer magnetic model is used to simulate the influence of such an alternance on the sea-surface magnetic anomalies. Conversely, observed magnetic profiles at the SWIR are modeled to unravel their off-axis crustal structure and past mode of spreading. The intruding gabbro bodies on the footwall of detachment faults play a major role in explaining the variability of sea-surface magnetic anomalies at slow and ultraslow spreading ridges.

Plain Language Summary Marine magnetic anomalies result from the capacity of oceanic crust to record the ambient geomagnetic field polarity at the time of its formation at mid-ocean ridges. These anomalies are usually well-defined on magmatic crust formed at faster spreading ridges, but they are more elusive on magma-poor crust of slower spreading ridges. Previous magnetic studies on the ultraslow spreading Southwest Indian Ridge show magnetic anomalies that are hardly identifiable on some segments. We investigate the hypothesis that the variability of the marine magnetic anomalies on this ridge results from the alternance of two modes of spreading. In the first one, seafloor spreading is achieved through the formation of magmatic crust, in the second one through detachment faulting which exhumes mantle rocks and intrusive gabbro bodies in a magma-poor environment. Serpentinized mantle does generally not record accurately the geomagnetic polarity, so magnetic anomalies over the detachment faults rely on the intrusive gabbro bodies, capable to record the magnetic polarity. The quality of the magnetic signal depends on the abundance of these gabbro bodies, which in turn reflects the local degree of magmatism. We use forward modeling to simulate and confirm these hypotheses and test their reliability on observed magnetic profiles.

1. Introduction

Magnetic studies at the Southwest Indian Ridge (SWIR) show that magnetic Chrons are scarcely identifiable in some areas (Bronner et al., 2014; Cannat et al., 1999; Patriat et al., 1997, 2008). One interpretation is that the ultraslow spreading rate shortens the intervals between adjacent magnetic polarity boundaries and makes them contaminate each other (Tivey & Tucholke, 1998). Another factor that may affect the anomalies at slow and ultraslow spreading centers is spreading through extension on detachment faults. The impact of detachment faults on marine magnetic anomalies tightly depends on the local degree of magmatism. The study of high-resolution deep-sea magnetic and bathymetric data at three oceanic core complexes (OCCs) shows that magmatism influences the structure and evolution of the OCCs, which in turn generates different magnetic anomalies (Zhou et al., in press). Sea-surface magnetics at the amagmatic easternmost SWIR display ubiquitously weak anomalies without any clear isochrons (Cannat et al., 2006; Sauter et al., 2008), whereas magnetic anomalies at the more magmatic segments near Atlantis II fracture zone (FZ) are readily defined even over detachment surfaces (Bronner et al., 2014; Hosford et al., 2003). In this study, we attempt to simulate the variability of sea-surface magnetic anomalies by using a three-layer magnetic crustal structure with variable degrees of magmatism. The forward modeling results indicate that seafloor spreading at detachment faults weakens or erases the magnetic anomalies at lower degrees of magmatism. When magmatism increases, intrusive gabbro bodies underlying the detachment footwall record the geomagnetic polarity and form clearer magnetic anomalies. Conversely, we

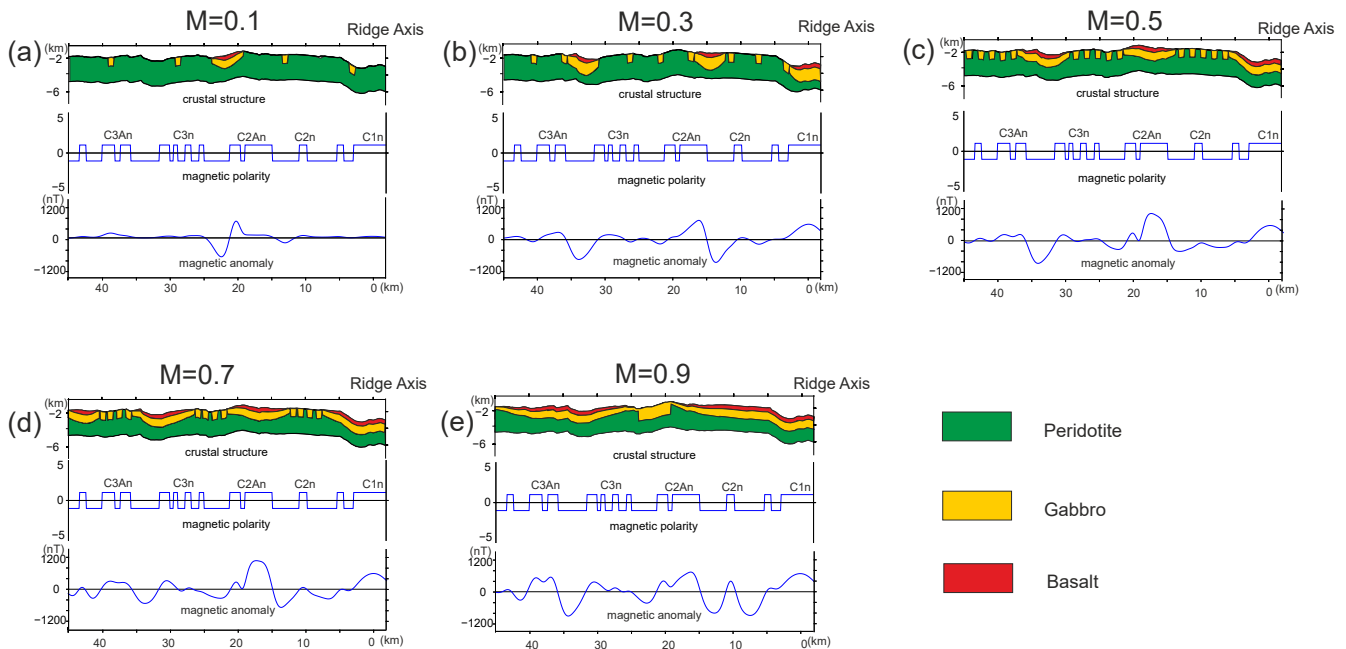


Figure 1. Forward modeling of off-axis magnetic profiles with different degrees of magmatism (M). For every panel, Top: Crustal structure; Middle: Geomagnetic polarity; Bottom: Modeled magnetic anomaly. See text for details on model parameters.

model the magnetic crustal structure along observed sea-surface magnetic profiles from segments of the SWIR showing different degrees of magmatism. This approach provides a new way to investigate the off-axis crustal structure from magnetics.

2. Method

In our model, sea-surface magnetic anomalies are assumed to arise from a 3 km magnetized layer made of basalt, gabbro, and serpentinized peridotite. For magmatic crust, the basalt, gabbro, and peridotite layers are 500 m, 1,500 m, and 1,000 m thick, respectively, whereas over detachment faults no basalt layer is considered and 1,000 m-thick gabbro bodies intrude into serpentinized peridotite within the detachment footwall. Basalt bears a strong remanent magnetization, gabbro an intermediate remanent magnetization, and serpentinized peridotite a low induced magnetization (15 A/m, 2 A/m, and 0.5 A/m, respectively, in the forward models of Figure 1). Intrusive gabbro within serpentinized peridotite on detachment faults bears a stronger magnetization reflecting their faster cooling rate at shallower depth (Hosford et al., 2003; 4 A/m in forward models of Figure 1).

After assigning the thickness and magnetization of every layer for each type of spreading (magmatic and along detachment faults), we laterally divide every layer into prisms (100 m wide in forward models of Figure 1). We compute the magnetic signal at each observation point by adding the contributions of all the three-layer prism units with different depth, thickness, and uniform magnetization. The contribution is calculated by using the formulas of (Bhattacharyya, 1964), assuming that each prism extends infinitely in the orthogonal direction (2D forward modeling).

For the forward modeling, we apply a constant half-spreading rate of 7 km/Myr and calculate the location of the geomagnetic polarity reversal boundaries, that is, the seafloor spreading Chrons, according to the timescale of Cande & Kent. (1995). Conversely, for the modeling of observed profiles we adjust the location of every Chron within a reasonable range to better fit the observed data and further calculate the spreading rate during each period.

3. Results

Parameters considered in this study include the ratio between detachment fault and magmatic crustal accretion and the thickness and magnetization of magnetized layers or gabbro bodies intruded into the detachment fault footwall. The local effects of alteration processes like maghemitization of titanomagnetite that decreases the magnetization of basalt (e.g., Tivey et al., 1993) and serpentinization that increases the magnetization of peridotite (e.g., Sztikar et al., 2014) at hydrothermal sites are not considered, because they generate a negligible signal on sea-surface magnetic data. We aim at investigating the effect of detachment faults on sea-surface magnetic anomalies, so the degree of magmatism M defined as the ratio of basalt exposure over the entire across-axis seafloor (Buck et al., 2005), the thickness and the magnetization of intrusive gabbro bodies in the detachment footwall are of primary concern.

3.1. Variation of Degree of Magmatism

The degree of magmatism M determines the modes of faulting on the seafloor, which in turn influence the expression of marine magnetic anomalies. As Figure 1 shows, we set up crustal models with M varying between 0.1, 0.3, 0.5, 0.7, and 0.9. The intrusive gabbro bodies are more abundant within the detachment fault footwall for higher M (Ciazela et al., 2015), as confirmed by two end-members, the more magmatic Atlantis Bank, where the whole footwall is made of gabbro (Dick et al., 2000), and the amagmatic easternmost SWIR, where only rare gabbro bodies are outcropping (Cannat et al., 2006; Sauter et al., 2013).

The results (Figure 1) show that, when the degree of magmatism and abundance of intrusive gabbro bodies increase, the forward reduced-to-the-pole magnetic anomaly better records the magnetic polarity. When $M = 0.1$ (Figure 1a), the oceanic crust is similar to the smooth seafloor, accommodated by detachment faults with seldom distributed gabbro bodies in the footwall. The succession of detachment faults with opposite polarity (Sauter et al., 2013) is occasionally interrupted by a transient magma pulse, creating a 0.1 fraction of magmatic seafloor. The forward magnetic anomaly shows that the magmatic crust undoubtedly recovers magnetic reversals with a satisfying shape and amplitude. Over detachment faults, the intrusive gabbro bodies formed within polarity intervals (e.g., C3An or C2r in Figure 1a) also recover the polarities with a lower amplitude, whereas the gabbro bodies formed during polarity reversals (e.g., young Matuyama and Jaramillo or C3n in Figure 1a) are not recorded well. Our simplifying assumptions consider only peridotite on the footwall, and therefore magnetic anomaly presents uniformly weak amplitude and no identifiable reversal even for long polarity intervals like C2An (Figure 1a).

When M increases to 0.3 (Figure 1b), the neo-volcanic zone forms a central magnetic anomaly within Brunhes (0–0.78 Ma). Again the magmatic crust reflects the magnetic polarity, for example, over C2r and C2An or on C3r. However, when reversals happen frequently in a series of short intervals as within C3n, the computed anomaly misses the detailed polarity sequence. The detachment footwall shows a similar signature as for $M = 0.1$. When $M = 0.5$ (Figure 1c), most of the polarity intervals are identified, especially over magmatic crust. The intruded gabbro bodies contribute enough for an easy recognition of the main Chrons, but the magnetic anomaly shows low amplitude and smooth shapes lacking details of the polarity sequence. In C3n, frequent polarity reversals occurring when a detachment fault is active results in improper recording of the polarity sequence by the detachment footwall, making the resulting magnetic anomaly quite flat. When M increases to 0.7 (Figure 1d), all magnetic anomalies are rather well recorded and display comparable amplitude to those over magmatic crust, even over detachment faults due to the more frequent gabbro bodies. Finally, when M reaches 0.9 (Figure 1e), the detachment footwall is overwhelmed by gabbro intrusions, so that all magnetic polarity intervals are well recovered even over the detachment fault.

3.2. Covariance of Parameters

These results show that the abundance of intrusive gabbro bodies is an essential parameter controlling the proper record of the magnetic polarity sequence. The amount of intrusive gabbro in the detachment footwall is determined by the given value of M , and so their intensity of magnetization and thickness decides on the capability of the crust to record the magnetic polarity reversals. We compute magnetic anomalies by using varying magnetization and thickness of the gabbro bodies for each degree of magmatism M and compare them quantitatively with

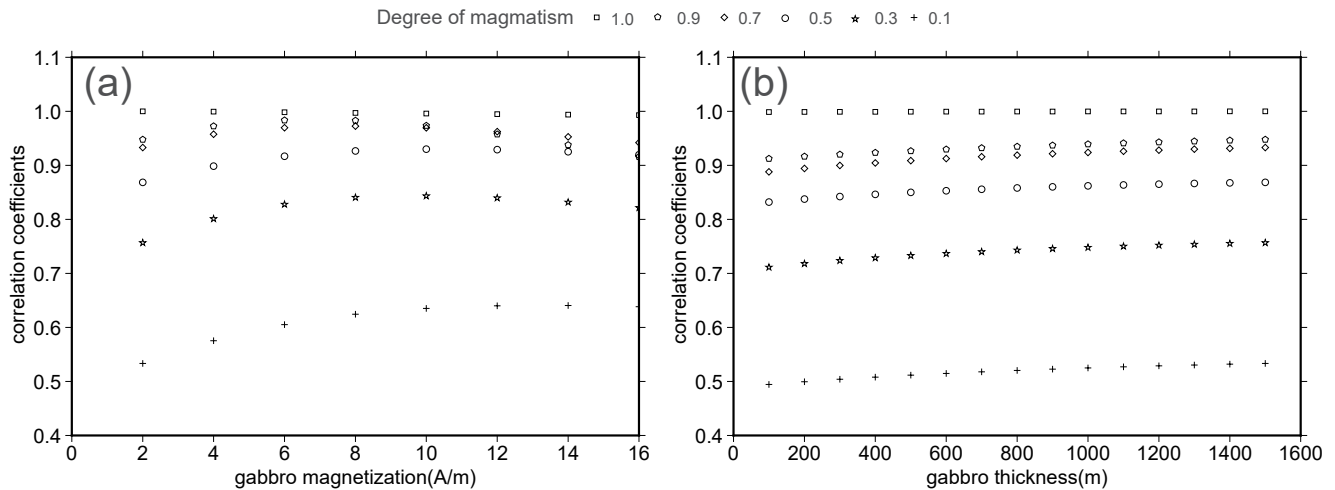


Figure 2. Correlation coefficients between the magnetic anomaly models for different degrees of magmatism M and the reference model (i.e., $M = 1$) for (a) varying gabbro magnetization and (b) varying thickness of the intrusive gabbro bodies.

the anomalies computed for a purely magmatic crust (i.e., the reference anomaly model) in order to obtain correlation coefficients. As Figure 2 shows, for a given magnetization and thickness, higher correlation coefficients are obtained for higher M , that is, more magmatic seafloor. In general, when $M \geq 0.7$, the magnetic anomalies present a strong correlation to the reference anomaly model, whereas when M is down to 0.1, no relation can even be inferred between this anomaly and the reference anomaly model. At a given degree of magmatism, the correlation coefficients only slightly increases when the thickness of the intrusive gabbro bodies increases from 100 to 1,500 m (Figure 2b). The variation of magnetization is more complicated, with the correlation increasing with gabbro magnetization at low values then, after a maximum (e.g., 10 A/m for $M = 0.3$ and 0.5 or 8 A/m for $M = 0.7$), decreasing above this value. This decreasing correlation may reflect the increasing contrast of magnetization between footwall gabbro bodies and serpentinite, whose contribution primarily depends on the gabbro body distribution.

3.3. Inverse Modeling of Observed Magnetic Anomaly Profiles

The previous forward modeling exercise shows us possible magnetic signatures associated with different geological patterns. (a) The magmatic crust properly records the shape and amplitude of the magnetic anomalies; (b) Detachment footwall exclusively made of serpentinitized peridotite does not properly record any magnetic anomaly; (c) The intrusive gabbro bodies beneath the detachment footwall have a variable capability to record magnetic anomalies depending on the degree of magmatism: the more magmatism, the better shape, and higher amplitude of the anomalies; (d) The conjunction of a polarity transition and a detachment footwall results in reduced amplitude of the main magnetic anomalies and eventual loss of short polarity events.

We can accordingly examine if the modeling method is able to infer the crustal structure of observed magnetic profiles. We assume the magnetization of gabbro to be 2 A/m in magmatic crust and 3 A/m when underlying a detachment fault, to reflect the faster cooling of the latter. Peridotite is assigned a low induced magnetization of 0.2 A/m. The dipole hypothesis applies for long periods and declination is not considered. Inclination is set to -75° , close to the -71° measured by paleomagnetism on drilling site 735B at Atlantis Bank (Dick et al., 2000). The magnetization of basalt near and far away from the ridge axis is adjusted to fit the observed anomalies. Once the type of crust and thickness of the various layers assigned, we adjust the polarity boundaries to better fit the forward-modeled magnetic anomaly to the observed one. We try to fulfill the condition that the full spreading rate of the SWIR should remain constant at ~ 14 km/Myr (Patriat et al., 1997, 2008), which means that a lower spreading rate on one flank should be compensated by a higher one on the conjugate flank.

Figure 3 shows four magnetic profiles located in different magmatic segments of the SWIR. After modeling the crustal structure of each profile, we estimate the degree of magmatism M (i.e., the ratio of magmatic crust along

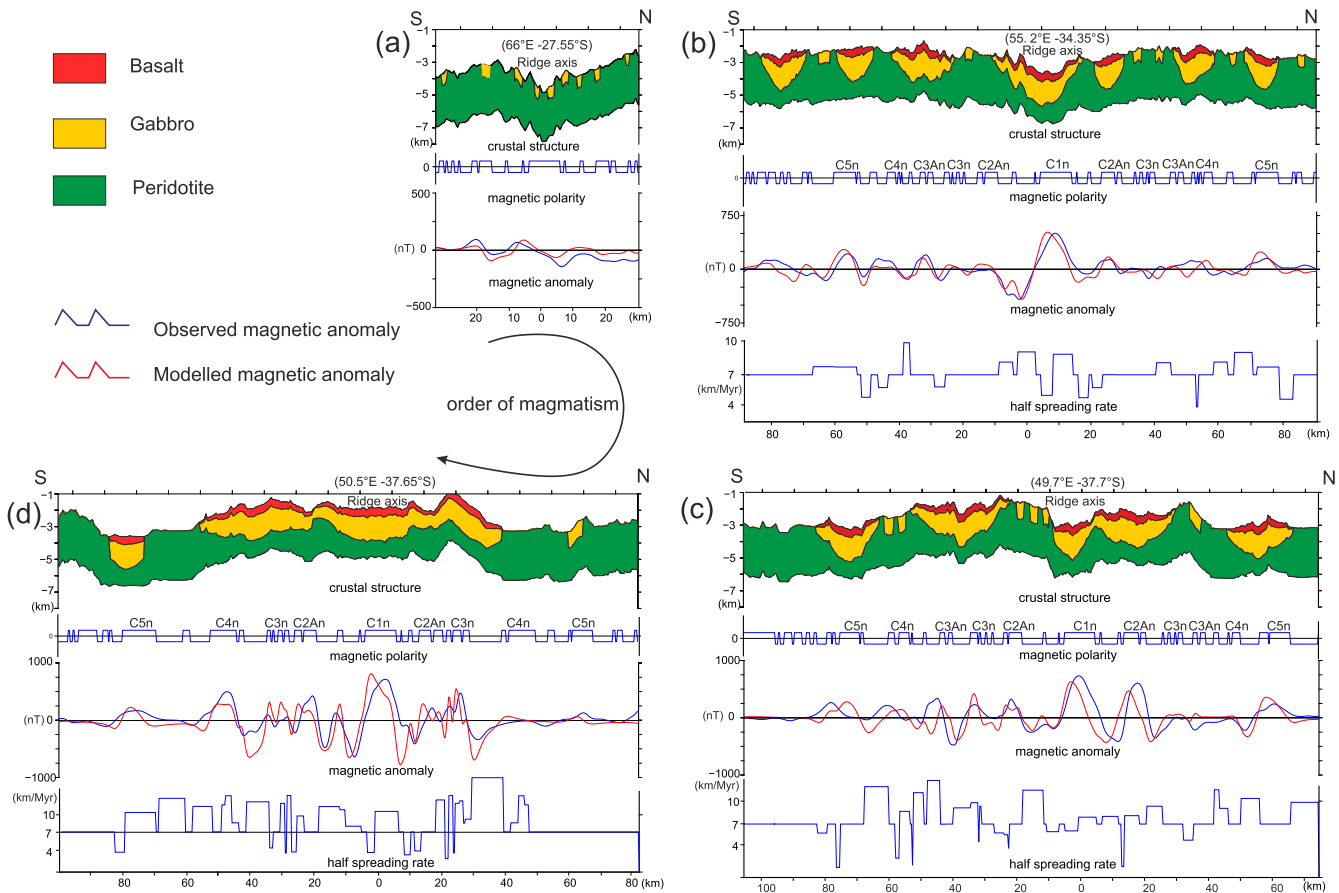


Figure 3. Modeling of observed magnetic profiles on several Southwest Indian Ridge segments with different degrees of magmatism. For every panel, Top: Deduced off-axis crustal structure from magnetic anomaly; Upper middle: Geomagnetic polarity. Lower middle: Modeled (red) and observed (blue) magnetic anomalies; Bottom: Calculated half spreading rate.

a profile over the entire length of the profile). Profiles on Figures 3a–3d span a wide range of M , from nearly zero to about one, corresponding to the variation of along-axis magma supply.

On Figure 3a (66°E), the easternmost SWIR displays detachment faults on both flanks (Cannat et al., 2006), observed magnetic anomalies (blue) show low amplitude (<200 nT), central magnetic anomaly is absent and no magnetic Chron can be identified. We therefore set up the model with only detachment footwall with a few gabbro intrusions under relatively higher amplitude magnetic anomalies. The computed magnetic anomaly (red) fits the observed anomaly well (blue), meaning that the model offers an acceptable solution although such a solution is intrinsically non-unique.

Further west (Figure 3b), the profile (55.2°E) lies between the Gallieni and Atlantis II FZs where several transform faults and large non-transform discontinuities separate the ridge into a series of short segments (Sauter et al., 2001, 2004). East of the Atlantis II FZ, Atlantis Bank is a large oceanic core complex on the footwall of which only gabbro was observed and drilled (Dick et al., 2000). The crustal accretion model is adjusted according to our relationship between magnetic anomalies and geological patterns. The strong central magnetic anomalies at the ridge axis and on Chron C5 should correspond to magmatic crust. The flat anomalies over Chron C2A on the southern flank are characteristic of reduced amplitude associated with detachment fault, and contrast with the broad positive anomaly reflecting magmatic crust on the conjugate northern flank. North of this magmatic crust, the magnetic anomaly shows near-zero amplitude except for a small oscillation over Chron C3n, so this accretion period is probably accommodated by a detachment fault with gabbro intrusions near C3n. On the conjugate southern flank, a broad C3n anomaly with low amplitude and a large C3An anomaly are observed, which correspond to a long period of magmatic spreading. We find accordingly that the crustal accretion deduced from magnetic anomalies in this region is similar to the evolution of the SWIR at 64°E, where the magmatic crust and

detachment fault spreading happen alternately on conjugate flanks (Searle & Bralee, 2007). Based on the same criteria, we assign magmatic crust during Chrons C4 and C5 on the northern flank with an intermediate episode of detachment accretion. On the conjugate southern flank, magmatic crust was formed during Chron C5 and was followed by a short period of detachment spreading. Magmatic crust corresponding to a broad anomaly was created during Chron C5A. Older off-axis crust displays weaker anomalies, because the magnetic minerals have been altered by pervasive hydrothermal circulation while the crust was progressively blanketed by sediments (e.g., Petersen et al., 1979; Tivey & Tucholke, 1998). These weaker anomalies, usually older than 10 Ma (Dyment et al., 2015), do not provide much constraints. The magnetization of basalt for this profile is set to 12 A/m and 3 A/m near and far away from the ridge axis, respectively. The estimated degree of magmatism M is 0.61 in this area, close to the range of values (0.3–0.5) favorable to the development of detachment faults obtained from numerical modeling (Tucholke et al., 2008). Figure 3b shows a maximum asymmetry of 29.5% between the two conjugate flanks.

The area between Indomed and Gallieni FZs displays the most magmatic segments of the SWIR, with the lowest mantle Bouguer gravity anomaly and $\text{Na}_{8,0}$ content in basalt samples, the highest amplitude of the central magnetic anomaly, and the thickest crust (Sauter & Cannat, 2010; Sauter et al., 2001). In this area, we select two sea-surface magnetic anomaly profiles, one (Figure 3c) across the Longqi OCC (Wu et al., 2021), and the other (Figure 3d) in the middle of magmatic spreading segment 27 (Chen et al., 2021). We construct the crustal accretion model for the western less magmatic area (Figure 3c). Over the Longqi OCC, on the southern flank, the magnetic anomaly shows low amplitude with a small peak corresponding to Chron C2n, which may be recorded by an intrusive gabbro body on the footwall of the detachment, whereas a large magnetic anomaly with amplitude comparable to that of the central magnetic anomaly C1n should be related to magmatic crust on the conjugate northern flank. With the same alternance, a long stripe of magmatic crust, corresponding to Chrons C2Ar to C4n, comes up on the southern flank and exhibits well-defined magnetic anomalies; a detachment fault is inferred on the northern flank, although its geometry departs from the typical detachment geometry (e.g., Smith et al., 2006). Chron C5 displays clear magnetic anomalies on both flanks, resulting from magmatic crust. Given the distribution of magmatic and tectonic crust, the degree of magmatism M is 0.63 in this region. The magnetization of basalt near and away from ridge axis is 15 A/m and 6 A/m, respectively. A large asymmetry of 77% is observed between Chrons C2 and C2A flank at the expense of the northern flank, corresponding to the development of the Longqi detachment fault on the southern flank. At that time magmatic spreading on the northern flank is slow, which probably means that most of the plate divergence was accommodated by the detachment fault during this period.

The last profile (Figure 3d) cuts across the most magmatic segment, which lacks the deep axial valley rift typical of the ultraslow spreading centers. The profile shows well-defined magnetic anomalies of strong amplitude from Chron C4 to the present. The crustal accretion during this period was fully accommodated by magmatic spreading. However, beyond a clear topographic step on both flanks at Chron C4, the magnetic anomaly shows a very low amplitude, with only one exception on the southern flank during Chron C5n which shows a magnetic anomaly comparable to that of the previous profile for the same age and flank (Figure 3c). Following our criteria, the crust older than Chron C4 should be formed by detachment fault spreading, with a transient magmatic crust at Chron C5n of the southern flank. The spreading mode of this segment before C4 (i.e., ~8 Ma) is similar to the amagmatic smooth seafloor (e.g., Figure 3a). After 8 Ma, a strong magmatic event happened in that area, which raised the topography, reduced the axial valley rift, and changed the spreading mode to fully magmatic. The resulting basalt magnetization is 10 A/m near the ridge axis (up to Chron C2A included) and 6 A/m further away. While there is no alternance between detachment fault and magmatic crust in this area, the predicted spreading rates display a significant asymmetry as high as 29.5% during Chron C4r.

4. Discussion

4.1. Magnetization and Thickness of the Different Sources

While modeling observed magnetic anomaly profiles with different degrees of magmatism, we assume similar thickness of the basalt and gabbro layers in the magmatic crust and fix the magnetization of gabbro to 2 A/m in the magmatic crust and 3 A/m under the footwall of detachment faults. Under these assumptions, we find that the magnetization of basalt cannot be kept constant if we try to properly adjust the amplitude of the observed anomalies. Across axis, basalt magnetization is stronger at the ridge axis and decreases off-axis due to the alteration of

titanomagnetite to the less-magnetic titanomaghemite (Irving, 1970; Johnson & Atwater, 1977), as it is observed globally (Dyment et al., 2015). Along-axis, the basalt magnetization also varies from 12 A/m at 55.2°E to 15 A/m at 49.7°E to 10 A/m at 50.5°E (Figures 3b–3d). The lower basalt magnetization on the 50.5°E profile (Figure 3d; Segment 27 of Sauter et al., 2004) with respect to the two other profiles (Figures 3b and 3c) probably reflects the higher degree of magmatism, which results in less fractionated basalt and a lower iron content (e.g., Hosford et al., 2003; Sempéré et al., 1995). As a confirmation, the SWIR axis in Segment 27 is underlain by a magma chamber (Jian et al., 2017). The different basalt magnetization shown by profiles at 55.2° and 49.7°E (Figures 3b and 3c) is more difficult to explain, because both areas show a similar degree of magmatism (~0.6). The difference may result from the lateral extent of the segments and observed anomalies: the 55.2°E segment (Segment 21 of [Sauter et al., 2004]) is narrow (35 km wide) and bounded by fracture zones, whereas the 49.7°E segment (Segment 28) is wider (55 km) and in direct continuation of segment 27 eastward. The difference of magnetization may just mark the shortcomings of the 2D assumption in our forward models.

Gabbro comes in two different settings, beneath basalt in normal magmatic crust and intruding the footwall of detachment faults. We assume that the latter bears a higher magnetization (3 A/m) than the former (2 A/m) due to faster cooling and higher fractionation at shallower depth (Allerton & Tivey, 2001; Pariso & Johnson, 1993). The contribution of gabbro to the sea-surface magnetic anomaly cannot be neglected, as it provides the longer wavelength magnetic anomalies on magmatic crust and most of the magnetic signal on the detachment footwall.

The contribution of serpentinized peridotite to the sea-surface magnetic anomaly is still controversial. Sauter et al. (2008) show that a 4 A/m remanent magnetization for serpentinized peridotite properly fits observed magnetic anomalies over corrugated and smooth seafloor. However, dredged samples show a low and variable Koenigsberger ratio (Remanent/Induced magnetizations) as a result of randomly oriented and magnetically unstable components leading to an incoherent natural remanent magnetization (NRM; Bronner et al., 2014; Maffione et al., 2014). Such a NRM would not significantly contribute to the sea-surface magnetic anomalies. These different interpretations again reflect the fundamental non-uniqueness of the potential field solutions. A more realistic crustal structure considers the contribution of both gabbro and serpentinized peridotite is constructed. In this three-layer model (basalt, gabbro, and serpentinite), we find that intrusive gabbro bodies underneath the detachment footwall can significantly contribute to the magnetic anomalies. These bodies are discontinuous, their interval depending on the degree of magmatism, which in turn create the important variability of the magnetic anomalies on the SWIR. We therefore do not need to assign a significant NRM to the serpentinized peridotite and only give it an induced magnetization of 0.2 A/m. We cannot exclude, however, that some anomalies ascribed to gabbro bodies may actually correspond to a patch of serpentinite bearing a strong NRM, although the occurrence of such patches and the law governing their distribution are still elusive.

As for the thickness of each magnetized layer, 500 m is generally adopted for the extrusive basalt layer of magmatic crust based on drilling results (Site 504B, e.g., [Becker et al., 1989]). The 1.5 and 1 km assigned to the gabbro for the magmatic crust and the detachment footwall may be thicker, to concur with the observation at drilling Site 735B (Dick et al., 2000), if a weaker magnetization is given to these magnetic sources. The adopted values represent a balance between thickness and magnetization.

4.2. Polarity and Spreading Rate

Although polarity reversals are almost instantaneous at geological scale (<6,000 years; e.g., Valet et al., 2012), the geometry of the polarity transition in the oceanic crust is complex and reflects the processes at work—piling of lavas of different viscosities on a smoother or rougher topography, injection of dykes within the neovolcanic zone, and progressive cooling of crystal mush to gabbro (e.g., Kidd, 1977). For instance, the polarity boundaries are dipping inward (i.e., toward the ridge axis) within the extrusive basalt, and outward within the gabbro layer (Macdonald et al., 1983). The cooling rate and the width of the transition zone also depend on the spreading rate. At the fast spreading East Pacific Rise, abundant low-viscosity lava spread over wide areas resulting in sub-horizontal polarity boundaries extending 7–8 km off-axis (Maher et al., 2021), whereas the axial valley walls restrict the flow of more viscous and less abundant lava at slow and ultraslow spreading ridges. As for dipping isotherms within the deeper crust, the faster cooling of exhumed gabbro at drilling Site 735B on Atlantis Bank suggests almost vertical polarity boundaries (Hosford et al., 2003). These remarks suggest that polarity transitions are generally narrow at ultraslow spreading centers. We therefore adopt vertical polarity boundaries for simplicity.

To fit the modeled magnetic anomaly with observed magnetic anomaly, we adjust the polarity intervals width and then calculate spreading rates within the different periods. The resulting spreading rates show strong, unrealistic variations, especially for the shorter intervals, reflecting uncertainties on the geomagnetic polarity time scale and the location of the polarity boundaries. We observe from Figures 3a–3d that profiles across the more magmatic segments require more adjustments to fit details of the measured anomalies. We suspect that it only reflects the higher resolution of the magmatic crust, recording all polarity reversals whereas the discontinuous gabbro bodies of the detachment footwall only provide a degraded version of the geomagnetic polarity time scale.

5. Conclusion

A three-layer model with detachment fault and intrusive gabbro bodies is proposed to approach the crustal structure at ultraslow spreading centers. Our forward modeling shows that the occurrence of detachment fault spreading may indeed distort the sea-surface magnetic signal and explain the variability of the observed anomalies. Gabbro plays an essential role in our model, especially over detachment footwalls where the intrusive gabbro bodies are the main source of the anomalies. With increasing degree of magmatism, the gabbro bodies beneath the detachment footwall become more frequent, resulting in a better record of the magnetic anomalies. The correlation coefficients obtained between magnetic anomalies modeled for different degrees of magmatism on one hand, and modeled for purely magmatic seafloor on the other hand, also demonstrate the importance of intrusive gabbro bodies to the anomalies. Conversely, inverse modeling of observed off-axis profiles with different degrees of magmatism on the SWIR shows that the type of seafloor spreading mode—magmatic or along detachment faults—at different periods can be deduced from the observed anomalies. Additional effects should however be considered as well, such as the alteration of the extrusive basalt and the consequent reducing magnetization with time, or the fractionation related to different degrees of magmatism which affects the iron content and the magnetization of extrusive basalt. The extreme variability of sea-surface magnetic anomalies related to seafloor spreading at ultraslow spreading centers may represent a tool for first-order estimate of the spreading mode over large areas, pending more detailed investigations.

Data Availability Statement

The magnetic data displayed in Figure 3 are available at NCEI (www.ngdc.noaa.gov/mgg/geodas/trackline.html). See also cruises RODRIGUEZ 2 (<http://doi.org/10.17600/84001211>) and GALLIENI (<http://doi.org/10.17600/95010090>) on the French Oceanographic Fleet web site.

Acknowledgments

We thank the crew and scientists of Cruises RODRIGUEZ 2 (1984; <http://doi.org/10.17600/84001211>) and GALLIENI (1995; <http://doi.org/10.17600/95010090>) for the magnetic data of Figure 3 (available at NCEI www.ngdc.noaa.gov/mgg/geodas/trackline.html). Fei Zhou is funded by China Scholarship Council (201906170047). We thank reviewers Tao Zhang and Maurice Tivey and Editor Monika Korte for their useful comments. This is IGP contribution 4260.

References

- Allerton, S., & Tivey, M. A. (2001). Magnetic polarity structure of the lower oceanic crust. *Geophysical Research Letters*, 28(3), 423–426. <https://doi.org/10.1029/2000GL008493>
- Becker, K., Sakai, H., Adamson, A. C., Alexandrovich, J., Alt, J. C., Anderson, R. N., et al. (1989). Drilling deep into young oceanic crust, Hole 504B, Costa Rica Rift. *Reviews of Geophysics*, 27(1), 79. <https://doi.org/10.1029/RG027i001p00079>
- Bhattacharyya, B. K. (1964). Magnetic anomalies due to prism-shaped bodies with arbitrary polarization. *Geophysics*, 29(4), 517–531. <https://doi.org/10.1190/1.1439386>
- Bronner, A., Sauter, D., Munsch, M., Carlot, J., Searle, R., Cannat, M., & Manatschal, G. (2014). Magnetic signature of large exhumed mantle domains of the Southwest Indian Ridge—Results from a deep-tow geophysical survey over 0 to 11 Ma old seafloor. *Solid Earth*, 5(1), 339–354. <https://doi.org/10.5194/se-5-339-2014>
- Buck, W. R., Lavier, L. L., & Poliakov, A. N. B. (2005). Modes of faulting at mid-ocean ridges. *Nature*, 434(7034), 719–723. <https://doi.org/10.1038/nature03358>
- Cande, S. C., & Kent, D. V. (1995). Revised calibration of the geomagnetic polarity timescale for the Late Cretaceous and Cenozoic. *Journal of Geophysical Research*, 100(B4), 6093–6095. <https://doi.org/10.1029/94JB03098>
- Cannat, M., Rommevaux-Jestin, C., Sauter, D., Deplus, C., & Mendel, V. (1999). Formation of the axial relief at the very slow spreading Southwest Indian Ridge (49° to 69°E). *Journal of Geophysical Research*, 104(B10), 22825–22843. <https://doi.org/10.1029/1999JB900195>
- Cannat, M., Sauter, D., Mendel, V., Ruellan, E., Okino, K., Escartin, J., et al. (2006). Modes of seafloor generation at a melt-poor ultraslow-spreading ridge. *Geology*, 34(7), 605–608. <https://doi.org/10.1130/G22486.1>
- Chen, J., Cannat, M., Tao, C., Sauter, D., & Munsch, M. (2021). 780 thousand years of upper-crustal construction at a melt-rich segment of the ultraslow spreading Southwest Indian Ridge 50°28'E. *Journal of Geophysical Research: Solid Earth*, 126(10), e2021JB022152. <https://doi.org/10.1029/2021JB022152>
- Ciazela, J., Koepke, J., Dick, H. J. B., & Muszynski, A. (2015). Mantle rock exposures at oceanic core complexes along mid-ocean ridges. *Geologos*, 21(4), 207–231. <https://doi.org/10.1515/logos-2015-0017>
- Dick, H. J. B., Natland, J. H., Alt, J. C., Bach, W., Bideau, D., Gee, J. S., et al. (2000). A long in situ section of the lower ocean crust: Results of ODP Leg 176 drilling at the Southwest Indian Ridge. *Earth and Planetary Science Letters*, 179(1), 31–51. [https://doi.org/10.1016/S0012-821X\(00\)00102-3](https://doi.org/10.1016/S0012-821X(00)00102-3)

- Dyment, J., Choi, Y., Hamoudi, M., Lesur, V., & Thebault, E. (2015). Global equivalent magnetization of the oceanic lithosphere. *Earth and Planetary Science Letters*, 430, 54–65. <https://doi.org/10.1016/j.epsl.2015.08.002>
- Hosford, A., Tivey, M., Matsumoto, T., Dick, H., Schouten, H., & Kinoshita, H. (2003). Crustal magnetization and accretion at the Southwest Indian Ridge near the Atlantis II fracture zone, 0–25 Ma. *Journal of Geophysical Research*, 108(B3), 2169. <https://doi.org/10.1029/2001JB000604>
- Irving, E. (1970). The Mid-Atlantic Ridge at 45°N. XIV. Oxidation and magnetic properties of basalt; review and discussion. *Canadian Journal of Earth Sciences*, 7(6), 1528–1538. <https://doi.org/10.1139/e70-144>
- Jian, H., Singh, S. C., Chen, Y. J., & Li, J. (2017). Evidence of an axial magma chamber beneath the ultraslow-spreading Southwest Indian Ridge. *Geology*, 45(2), 143–146. <https://doi.org/10.1130/G38356.1>
- Johnson, H. P., & Atwater, T. (1977). Magnetic study of basalts from the Mid-Atlantic Ridge, lat 37°N. *Geological Society of America Bulletin*, 88(5), 637–647. [https://doi.org/10.1130/0016-7606\(1977\)88<637:MSOBT>2.0.CO;2](https://doi.org/10.1130/0016-7606(1977)88<637:MSOBT>2.0.CO;2)
- Kidd, R. G. W. (1977). A model for the process of formation of the upper oceanic crust. *Geophysical Journal International*, 50(1), 149–183. <https://doi.org/10.1111/j.1365-246X.1977.tb01328.x>
- Macdonald, K. C., Miller, S. P., Luyendyk, B. P., Atwater, T. M., & Shure, L. (1983). Investigation of a Vine-Matthews Magnetic Lineation from a submersible: The source and character of marine magnetic anomalies. *Journal of Geophysical Research*, 88(B4), 3403. <https://doi.org/10.1029/JB088iB04p03403>
- Maffione, M., Morris, A., Plümpner, O., & van Hinsbergen, D. J. J. (2014). Magnetic properties of variably serpentinized peridotites and their implication for the evolution of oceanic core complexes. *Geochemistry, Geophysics, Geosystems*, 15(4), 923–944. <https://doi.org/10.1002/2013GC004993>
- Maher, S. M., Gee, J. S., Cheadle, M. J., & John, B. E. (2021). Three-dimensional magnetic stripes require slow cooling in fast-spread lower ocean crust. *Nature*, 597(7877), 511–515. <https://doi.org/10.1038/s41586-021-03831-6>
- Pariso, J. E., & Johnson, H. P. (1993). Do lower crustal rocks record reversals of the Earth's magnetic field? Magnetic petrology of oceanic gabbros from Ocean Drilling Program hole 735B. *Journal of Geophysical Research*, 98, 16013. <https://doi.org/10.1029/93JB00933>
- Patriat, P., Sauter, D., Munsch, M., & Parson, L. (1997). A survey of the Southwest Indian Ridge axis between Atlantis II Fracture Zone and the Indian Ocean Triple Junction: Regional setting and large scale segmentation. *Marine Geophysical Researches*, 19(6), 457–480. <https://doi.org/10.1023/A:1004312623534>
- Patriat, P., Sloan, H., & Sauter, D. (2008). From slow to ultraslow: A previously undetected event at the Southwest Indian Ridge at ca. 24 Ma. *Geology*, 36(3), 207–210. <https://doi.org/10.1130/G24270A.1>
- Petersen, N., Eisenach, P., & Bleil, U. (1979). Low temperature alteration of the magnetic minerals in ocean floor basalts. In M. Talwani, C. G. Harrison, & D. E. Hayes (Eds.), *Maurice Ewing Series* (Vol. 2, pp. 169–209). American Geophysical Union. <https://doi.org/10.1029/ME002p0169>
- Sauter, D., & Cannat, M. (2010). The ultraslow spreading Southwest Indian Ridge. In P. A. Rona, C. W. Devey, J. Dyment, & B. J. Murton (Eds.), *Geophysical Monograph Series* (Vol. 188, pp. 153–173). American Geophysical Union. <https://doi.org/10.1029/2008GM000843>
- Sauter, D., Cannat, M., & Mendel, V. (2008). Magnetization of 0–26.5 Ma seafloor at the ultraslow spreading Southwest Indian Ridge, 61°–67°E. *Geochemistry, Geophysics, Geosystems*, 9(4), Q04023. <https://doi.org/10.1029/2007GC001764>
- Sauter, D., Cannat, M., Rouméjon, S., Andreani, M., Birot, D., Bronner, A., et al. (2013). Continuous exhumation of mantle-derived rocks at the Southwest Indian Ridge for 11 million years. *Nature Geoscience*, 6(4), 314–320. <https://doi.org/10.1038/ngeo1771>
- Sauter, D., Carton, H., Mendel, V., Munsch, M., Rommevaux-Jestin, C., Schott, J.-J., & Whitechurch, H. (2004). Ridge segmentation and the magnetic structure of the Southwest Indian Ridge (at 50°30'E, 55°30'E and 66°20'E): Implications for magmatic processes at ultraslow-spreading centers. *Geochemistry, Geophysics, Geosystems*, 5(5), Q05K08. <https://doi.org/10.1029/2003GC000581>
- Sauter, D., Patriat, P., Rommevaux-Jestin, C., Cannat, M., & Briais, A. (2001). The Southwest Indian Ridge between 49°15'E and 57°E: Focused accretion and magma redistribution. *Earth and Planetary Science Letters*, 192(3), 303–317. [https://doi.org/10.1016/S0012-821X\(01\)00455-1](https://doi.org/10.1016/S0012-821X(01)00455-1)
- Searle, R. C., & Bralée, A. V. (2007). Asymmetric generation of oceanic crust at the ultra-slow spreading Southwest Indian Ridge, 64°E. *Geochemistry, Geophysics, Geosystems*, 8(5), Q05015. <https://doi.org/10.1029/2006GC001529>
- Sempéré, J. C., Blondel, P., Briais, A., Fujiwara, T., Géli, L., Isezaki, N., et al. (1995). The Mid-Atlantic Ridge between 29°N and 31°30'N in the last 10 Ma. *Earth and Planetary Science Letters*, 130(1–4), 45–55. [https://doi.org/10.1016/0012-821X\(94\)00259-2](https://doi.org/10.1016/0012-821X(94)00259-2)
- Smith, D. K., Cann, J. R., & Escartin, J. (2006). Widespread active detachment faulting and core complex formation near 13°N on the Mid-Atlantic Ridge. *Nature*, 442(7101), 440–443. <https://doi.org/10.1038/nature04950>
- Szitkar, F., Dyment, J., Fouquet, Y., Honscho, C., & Horen, H. (2014). The magnetic signature of ultramafic-hosted hydrothermal sites. *Geology*, 42(8), 715–718. <https://doi.org/10.1130/G35729.1>
- Tivey, M. A., Rona, P. A., & Schouten, H. (1993). Reduced crustal magnetization beneath the active sulfide mound, TAG hydrothermal field, Mid-Atlantic Ridge at 26°N. *Earth and Planetary Science Letters*, 115(1–4), 101–115. [https://doi.org/10.1016/0012-821X\(93\)90216-V](https://doi.org/10.1016/0012-821X(93)90216-V)
- Tivey, M. A., & Tucholke, B. E. (1998). Magnetization of 0–29 Ma ocean crust on the Mid-Atlantic Ridge, 25°30' to 27°10'N. *Journal of Geophysical Research*, 103(B8), 17807–17826. <https://doi.org/10.1029/98JB01394>
- Tucholke, B. E., Behn, M. D., Buck, W. R., & Lin, J. (2008). Role of melt supply in oceanic detachment faulting and formation of megamullions. *Geology*, 36(6), 455–458. <https://doi.org/10.1130/G24639A.1>
- Valet, J. P., Fournier, A., Courtillot, V., & Herrero-Bervera, E. (2012). Dynamical similarity of geomagnetic field reversals. *Nature*, 490(7418), 89–93. <https://doi.org/10.1038/nature11491>
- Wu, T., Tivey, M. A., Tao, C., Zhang, J., Zhou, F., & Liu, Y. (2021). An intermittent detachment faulting system with a large sulfide deposit revealed by multi-scale magnetic surveys. *Nature Communications*, 12(1), 5642. <https://doi.org/10.1038/s41467-021-25880-1>
- Zhou, F., Dyment, J., Tao, C., & Wu, T. (in press). Magmatism at oceanic core complexes on the ultraslow Southwest Indian Ridge: Insights from near-seafloor magnetics. *Geology*.